**Transactions of JASCOME Vol. 20 (Dec.), Paper No. 03-201219** JASCOME

# Topology optimization for unsteady flow using lattice kinetic scheme

Suqiong XIE[1)], Hiroshi ISAKARI[2)], Toru TAKAHASHI[3)], Toshiro MATSUMOTO[4)]

1) Nagoya University (Furo-cho, Chikusa-ku, Nagoya, Aichi, 464-8601, E-mail: xiesuqiong@nuem.nagoya-u.ac.jp)
2) Nagoya University (Furo-cho, Chikusa-ku, Nagoya, Aichi, 464-8601, E-mail: isakari@nuem.nagoya-u.ac.jp)
3) Nagoya University (Furo-cho, Chikusa-ku, Nagoya, Aichi, 464-8601, E-mail: ttaka@nuem.nagoya-u.ac.jp)
4) Nagoya University (Furo-cho, Chikusa-ku, Nagoya, Aichi, 464-8601, E-mail: t.matsumoto@nuem.nagoya-u.ac.jp)

This paper presents a topology optimization method for unsteady incompressible viscous fluid flow employing the lattice kinetic scheme as the solver of Navier-Stokes equations. The lattice kinetic scheme merges the lattice Boltzmann method with the kinetic schemes, hence it uses less computer memory and has a simpler boundary condition compared to the lattice Boltzmann method. This study considers an optimization problem of maximizing the dissipation kinetic energy of unsteady flow and aims at providing a solution to the design of hydraulic anti-vibration devices. The optimization is performed based on the gradient of the objective functional with respect to design variables. The design sensitivity is derived via the adjoint method. Numerical experiments are presented to confirm the validity of design sensitivity and the utility of the proposed method.

***Key Words***: Topology optimization, Lattice kinetic scheme, Unsteady flow, Dissipation kinetic energy

## 1. Introduction

The topology optimization methodology is a significant design tool for a variety of structural mechanics and is able to obtain optimal solutions through simulation techniques. In recent years, topology optimization has gained increasing attention and has been applied for solving various physical problems including fluid flow problems. Since Borrvall and Petersson first applied topology optimization to Stokes flow,[(1)] additional researches have extended its applications to different fluid flow such as laminar Navier-Stokes fluid flow[(2)] and various fluid devices like microfluidic mixers.[(3, 4)]

In the majority of previous studies, the Navier-Stokes equations are numerically solved for fluid simulation. In recent decades, the lattice Boltzmann method has become a popular solver of Navier-Stokes equations since it has a simple algorithm and does not need iterative computation to obtain macroscopic variables of fluid, thus it is easy to implement parallel computation and can save computational cost. In the lattice Boltzmann method, the lattice Boltzmann equation is a discretized Boltzmann equation that describes the time evolution of particle velocity distribution function. The particle velocity distribution function represents the probable number of particles at a point in the fluid field. In the kinetic theory, the particles are imaged to be in random motion, however, the lattice Boltzmann method approximately restricts the particles' velocity in finite directions and the macroscopic fluid variables, such as density, velocity, and pressure are able to be obtained from the discretized distribution functions.

After the pioneering study of applying the lattice Boltzmann method to topology optimization of fluid,[(5)] it has been employed in various studies of topology optimization for fluid flow problems.[(4, 6, 7)] However, the storage requirement remains a problem when the design domain includes a large number of grids since it is necessary to save the discretized distribution functions of every grid. In 2002, Inamuro proposed the lattice kinetic scheme,[(8)] which simplified the lattice Boltzmann equation by using a unit relaxation time and employs the Chapman-Enskog equilibrium distribution function,[(9, 10, 11)] Due to this change, the lattice kinetic scheme does not need to compute and save the discretized distribution functions of every grid; hence, it is able to save memory

Received Oct. 6, 2020, accepted Nov. 10, 2020

usage than the lattice Boltzmann method. In addition, the no-slip boundary can be directly imposed in the lattice kinetic scheme while the bounce-back condition must be considered in the lattice Boltzmann method. In this study, we employ the lattice kinetic scheme to simulate the unsteady fluid flow and use a new lattice Boltzmann equation to reduce the compressible effects following the research by He et al.[12]

Topology optimization for steady flow problems were primarily considered in previous researches. However, unsteady flows dominate many systems in reality, thus it is of great importance to develop a topology optimization method for unsteady flows. There are a number of researches studying topology optimization for unsteady flow problems employing the finite element method [13, 14] and the lattice Boltzmann method.[15, 16, 17] In this study, we consider a topology optimization method for unsteady flow using the lattice kinetic scheme. Conventionally, the problem of minimizing dissipation kinetic energy is commonly considered. This study focuses on solving the problem of maximizing dissipation kinetic scheme and aims at proposing a solution to the design of hydraulic anti-vibration systems.[18, 19, 17]

The adjoint method is an important tool in topology optimization since it is efficient to obtain the gradient of a cost function. In this study, according to the method proposed by Yaji et al.,[20] the adjoint function of lattice kinetic scheme is derived to compute the design sensitivity. The level set method is adopted in this study using the level set function to express the material distribution, which is updated by the time evolution level set function during the optimization.

In the rest of this article, we introduce the formulation of the optimization problem in Section 2, and in Section 4, numerical examples are presented for the validation of the proposed topology optimization method.

## 2. Problem formulation

### 2.1. Cost function

We consider the maximization of dissipation kinetic energy of an unsteady flow. The design domain is as shown in Fig. 1, where $D$ represents the design domain, $\Omega$, $\partial\Omega$ and $\bar{\Omega}$ represent the fluid domain, boundary of fluid domain and the solid domain, respectively; $\Gamma_{\mathrm{v}}, \Gamma_{\mathrm{p}}$ and $\Gamma_{\mathrm{w}}$ denote the velocity prescribed boundary, the pressure prescribed boundary and the wall of the design domain, respectively.

The objective functional is defined by adding a minus sign to the dissipation kinetic energy as follows:

$$\inf_{\phi} \quad J = -\int_I \int_D Z \mathrm{d}\Omega \mathrm{d}t, \tag{1}$$

$$\text{s.t.} \quad V = V_\Omega - V_{\max} \leq 0, \tag{2}$$

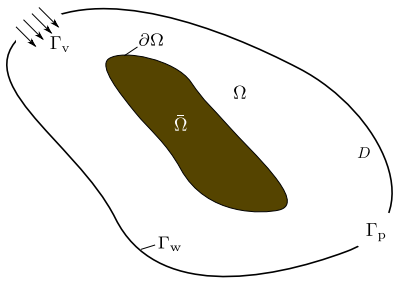

Fig. 1 Design domain.

where $Z$ calculates the dissipation kinetic energy by

$$Z = \frac{1}{2Re}(\nabla \boldsymbol{u} + \nabla \boldsymbol{u}^{\mathrm{T}}) : (\nabla \boldsymbol{u} + \nabla \boldsymbol{u}^{\mathrm{T}}), \tag{3}$$

and $J$ is the objective functional integrating $Z$ over $\Omega$ and time $I, t \in I$. $V \leq 0$ represents the volume constraint, $V_\Omega$ denotes the volume of fluid field and $V_{\max}$ denotes the allowed maximum volume of fluid field. $Re$ is the Reynolds number.

### 2.2. Lattice kinetic scheme

In this study, we use dimensionless variables defined by a characteristic length $\hat{L}$, a characteristic particle speed $\hat{c}$, a characteristic time scale $\hat{t}_0 = \hat{L}/\hat{U}$, where $\hat{U}$ is a characteristic flow speed, and a reference density $\hat{\rho}_0$.

Since lattice kinetic scheme is an extended lattice Boltzmann method, we introduce lattice Boltzmann method firstly in this section. The Boltzmann equation with the Bhatnagar-Gross-Krook collision operator is written as

$$\frac{\partial f}{\partial t} + \boldsymbol{c} \cdot \nabla f = -\frac{1}{\tau}(f - f^{\mathrm{eq}}), \tag{4}$$

where $f$ and $f^{\mathrm{eq}}$ are the particle velocity distribution function and the local equilibrium distribution function, respectively. The relaxation time $\tau$ is a parameter of $O(1)$. The lattice Boltzmann equation is a discretized Boltzmann equation reads

$$\begin{aligned} f_i(\boldsymbol{x}, t + \Delta t) =& f_i(\boldsymbol{x} - \boldsymbol{c}_i \Delta x, t) - \frac{1}{\tau}\left[f_i(\boldsymbol{x} - \boldsymbol{c}_i \Delta x, t)\right. \\ & \left. - {f_i}^{\mathrm{eq}}(\boldsymbol{x} - \boldsymbol{c}_i \Delta x, t)\right], \end{aligned} \tag{5}$$

where $f_i(\boldsymbol{x}, t)$ is the discretized distribution function $f$ representing the probable number of particles that moves in the direction $i$ at the point $\boldsymbol{x}$ and time $t$. $f_i^{\mathrm{eq}}$ is the discretized equilibrium function $f^{\mathrm{eq}}$. $\Delta x$ and $\Delta t$ represent the lattice length and step size, respectively. $\Delta t$ is chosen so that the particles travel one lattice spacing during the step size.

In the lattice Boltzmann method, the macroscopic fluid

parameters are computed by

$$\rho(\boldsymbol{x},t)=\sum_{i=1}^{N} f_i(\boldsymbol{x},t),$$
$$\rho\boldsymbol{u}(\boldsymbol{x},t)=\sum_{i=1}^{N} \boldsymbol{c}_i f_i(\boldsymbol{x},t),$$
$$p(\boldsymbol{x},t)=\frac{1}{3}\rho(\boldsymbol{x},t),$$

where $N$ is the number of discretized directions, $\rho$ and $p$ are the density and pressure of the fluid.

Inamuro [8] proposed the lattice kinetic scheme by setting $\tau=1$, so that Eq. (5) becomes

$$f_i(\boldsymbol{x},t+\Delta t)=f_i{}^{\mathrm{eq}}(\boldsymbol{x}-\boldsymbol{c}_i\Delta x,t), \tag{6}$$

and the equilibrium equation $f_i^{\mathrm{eq}}$ is defined as

$$f_i^{\mathrm{eq}}=w_i\rho\left\{1+3c_{i\gamma}u_\gamma+\frac{9}{2}c_{i\gamma}c_{i\beta}u_\gamma u_\beta-\frac{3}{2}u_\gamma u_\gamma +A\Delta x\left(\frac{\partial u_\beta}{\partial x_\gamma}+\frac{\partial u_\gamma}{\partial x_\beta}\right)c_{i\gamma}c_{i\beta}\right\}, \tag{7}$$

where $\beta$ and $\gamma=x$ or $y$ represents a component of Cartesian coordinates, where the summation convention is applied for repeated indices, and $w_i$ is the weight coefficient. $A$ is a constant parameter of $O(1)$, determining the kinetic coefficient $\nu$ of the fluid by

$$\nu=\left(\frac{1}{6}-\frac{2}{9}A\right)\Delta x.$$

Then, the macroscopic variables of the fluid can be computed as follows:

$$\rho(\boldsymbol{x},t)=\sum_{i=1}^{N} f_i^{\mathrm{eq}}(\boldsymbol{x}-\boldsymbol{c}_i\Delta x,t-\Delta t),$$
$$\rho\boldsymbol{u}(\boldsymbol{x},t)=\sum_{i=1}^{N} \boldsymbol{c}_i f_i^{\mathrm{eq}}(\boldsymbol{x}-\boldsymbol{c}_i\Delta x,t-\Delta t),$$
$$p=\frac{1}{3}\sum_{i=1}^{N} f_i^{\mathrm{eq}}(\boldsymbol{x}-\boldsymbol{c}_i\Delta x,t-\Delta t).$$

In the lattice kinetic scheme, $\boldsymbol{u}$, $\rho$ and $p$ can be computed from $f_i^{\mathrm{eq}}$ without using $f_i$. Therefore, $f_i, i=1,...,N$ does not need to be computed or saved.

Various lattice models of the lattice Boltzmann method have been proposed so far in the previous studies, among which the D2V9 model has been commonly used for two dimensional problems. In this research, we employ the D2V9 model, being shown in Fig. 2, which restricts the particles' velocity in 9 directions in the plane space, i.e., $N=9$. In the D2V9 model, the velocity vectors $\boldsymbol{c}_{i=1,...,9}$ of the particles are defined as

$$[\boldsymbol{c}_1,\boldsymbol{c}_2,\boldsymbol{c}_3,\boldsymbol{c}_4,\boldsymbol{c}_5,\boldsymbol{c}_6,\boldsymbol{c}_7,\boldsymbol{c}_8,\boldsymbol{c}_9] =\begin{bmatrix} 0 & 1 & 0 & -1 & 0 & 1 & -1 & -1 & 1\\ 0 & 0 & 1 & 0 & -1 & 1 & 1 & -1 & -1 \end{bmatrix},$$

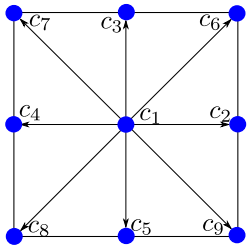

Fig. 2 D2V9 model

and the weight coefficients $w_i$ are given as

$$w_i=\begin{cases}\frac{4}{9} & i=1\\ \frac{1}{9} & i=2,3,4,5\\ \frac{1}{36} & i=6,7,8,9.\end{cases}$$

In the research by He et al. [12], a new lattice Boltzmann method is proposed for the reduction of the compressible influence in solving the Navier-Stokes equations. In this new lattice Boltzmann method, the fluid density is treated as a constant. Following this research, we have $f_i^{\mathrm{eq}}$ in the form as

$$f_i^{\mathrm{eq}}=w_i\left\{3p+\rho_0\left[3c_{i\gamma}u_\gamma+\frac{9}{2}c_{i\gamma}c_{i\beta}u_\gamma u_\beta-\frac{3}{2}u_\gamma u_\gamma\right.\right. \tag{8}$$
$$\left.\left.+A\Delta x\left(\frac{\partial u_\beta}{\partial x_\gamma}+\frac{\partial u_\gamma}{\partial x_\beta}\right)c_{i\gamma}c_{i\beta}\right]\right\}. \tag{9}$$

Consequently, $\boldsymbol{u}$ and $p$ are defined as

$$p(\boldsymbol{x},t)=\frac{1}{3}\sum_{i=1}^{N} f_i^{\mathrm{eq}}(\boldsymbol{x}-\boldsymbol{c}_i\Delta x,t-\Delta t),$$
$$\rho_0\boldsymbol{u}(\boldsymbol{x},t)=\sum_{i=1}^{N} \boldsymbol{c}_i f_i^{\mathrm{eq}}(\boldsymbol{x}-\boldsymbol{c}_i\Delta x,t-\Delta t).$$

In this study, $\rho_0$ is given as $\rho_0=1$. The first derivative $\frac{\partial u_\beta}{\partial x_\gamma}$ in Eq. (9) is calculated via the finite-difference approximation [8], expressed as

$$\frac{\partial u_\beta}{\partial x_\gamma}\approx\frac{1}{6\Delta x}\sum_{i=1}^{9} c_{i\gamma}u_\beta(\boldsymbol{x}+\boldsymbol{c}_i\Delta x).$$

### 2.3. Boundary conditions

The boundary conditions are summarized as follows:

$$\boldsymbol{u}=(U,0) \quad \text{on } \Gamma_{\mathrm{v}},$$
$$p=P \quad \text{on } \Gamma_{\mathrm{p}},$$
$$\boldsymbol{u}=\boldsymbol{0} \quad \text{on } \Gamma_{\mathrm{w}}.$$

In the lattice kinetic scheme, the macroscopic variables are directly specified at the boundaries, while the bounce-back boundary conditions in terms of the velocity distribution function should be applied in lattice Boltzmann method. Therefore, the additional advantage of lattice kinetic scheme is that we can use the same boundary conditions as those in the usual CFD simulations.

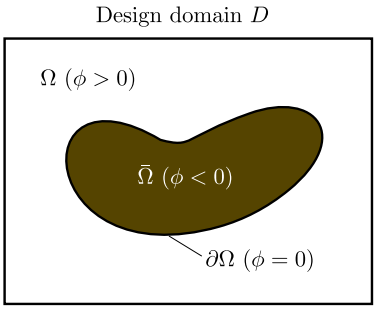


Fig. 3 Level set method

### 2.4. Level set method

In the level set method, a scalar function $\phi$, called level set function, is employed to distinguish the fluid and solid domain, which is defined as

$$\begin{cases} 0 < \phi(\boldsymbol{x}) \leq 1 & \text{if} \quad \boldsymbol{x} \in \Omega \\ \phi(\boldsymbol{x}) = 0 & \text{if} \quad \boldsymbol{x} \in \partial\Omega \\ -1 \leq \phi(\boldsymbol{x}) < 0 & \text{if} \quad \boldsymbol{x} \in \bar{\Omega}. \end{cases} \tag{10}$$

The characteristic function [21] $\chi_\phi$ is defined as

$$\chi_\phi(\boldsymbol{x}) = \begin{cases} 1 & \text{if} \quad \phi(\boldsymbol{x}) \geq 0 \Leftrightarrow \boldsymbol{x} \in \Omega \\ 0 & \text{if} \quad \phi(\boldsymbol{x}) < 0. \Leftrightarrow \boldsymbol{x} \in \bar{\Omega} \end{cases} \tag{11}$$

The volume of the fluid field is then calculated by

$$V_\Omega = \int_D \chi_\phi \mathrm{d}\Omega.$$

According to the research by Yamada et al. [21], the following reaction-diffusion equation is used to update $\phi$ during the optimization

$$\frac{\partial \phi}{\partial \zeta} = -K(J' - \tau_{\mathrm{R}} \nabla^2 \phi), \tag{12}$$

where $\zeta$ is fictitious time, $K > 0$ is a constant, $J'$ denotes the design sensitivity. $\tau_R \nabla^2 \phi$ is the regularization term controlling the complexity of the fluid domain shape. The boundary of the fluid domain can be extracted from the zero iso-surface of $\phi$. The boundary shape is changed in accordance with the update of the distribution of the value of $\phi$ during the optimization.

### 2.5. Sensitivity analysis

Yaji et al. [20] proposed a level set-based topology optimization method, in which the LSF $\phi$ is introduced to the lattice Boltzmann equation by replacing $\boldsymbol{u}$ with $\phi\boldsymbol{u}$ as below:

$$\boldsymbol{u} := \phi \boldsymbol{u},$$

and the design sensitivity is derived via the adjoint method. Following the research by Yaji et al. [21], we define the augmented objective functional $\bar{J}$ as follows:

$$\begin{aligned} &\bar{J} = J + G + \lambda V, \\ &G = \int_D \int_I \int_{\mathbb{R}} \tilde{f} \left[ \frac{\partial f}{\partial t} - \boldsymbol{c} \cdot \nabla f + \frac{1}{\tau}(f - f^{\mathrm{eq}}) \right] \mathrm{d}\boldsymbol{c}\mathrm{d}D\mathrm{d}t = 0, \end{aligned} \tag{13}$$

where $G$ is the constraint condition, $\mathbb{R}$ is the velocity space, $\tilde{f}(\boldsymbol{x}, \boldsymbol{c}, t)$ and $\lambda$ are the Lagrangian multipliers, $\lambda \geq 0$. Following Yaji et al. [20], we derive $\tilde{f}$ from the continuous Boltzmann equation and then discretize it using lattice kinetic scheme.

From the stationary state of $\bar{J}$, we have

$$\delta_f J + \delta_f G = 0,$$

where $\delta_f J$ and $\delta_f G$ denote the variations of $J$ and $G$ with respect to $f$. In this research, $\tilde{f}$ is derived as

$$\begin{aligned} &\tilde{f}_i(\boldsymbol{x} - \boldsymbol{c}_i \Delta \boldsymbol{x}, t - \Delta t) = \tilde{f}_i^{\mathrm{eq}}(\boldsymbol{x}, t) - Z', \\ &\tilde{f}_i^{\mathrm{eq}} = \sum_{j=1}^{9} \tilde{f}_j f_j^{\mathrm{a}} \left\{ 1 + 3(\boldsymbol{c}_i - \boldsymbol{u}) \cdot (\boldsymbol{c}_j - \boldsymbol{u}) \right\}. \end{aligned} \tag{14}$$

$\tilde{f}$ has the similar form with lattice Boltzmann equation and it is a backward problem, $\tilde{f}$ is called the adjoint function of $f$. In Eq. (14), $f_i^{\mathrm{a}}, (i = 1, ..., 9)$, $Z'$ are defined as

$$\begin{aligned} &f_i^{\mathrm{a}} = w_i(3p + \rho_0(3c_{i\gamma}u_\gamma + \frac{9}{2}c_{i\gamma}c_{i\beta}u_\gamma u_\beta - \frac{3}{2}u_\gamma u_\gamma). \\ &Z' = \delta_{f_i} J. \end{aligned}$$

Consequently, the design sensitivity is derived as

$$\begin{aligned} \delta_\phi \bar{J} = \int_D \Bigg\{ \int_I \Bigg[ \sum_{i=1}^{9} \tilde{f}_i 3 w_i (3p + \rho_0 (3 c_{i\gamma} u_\gamma + \frac{9}{2} c_{i\gamma} c_{i\beta} u_\gamma u_\beta \\ - \frac{3}{2} u_\gamma u_\gamma)(u_\gamma u_\gamma - c_{i\gamma} u_\gamma) \Bigg] \mathrm{d}t + \lambda \Bigg\} \delta\phi \mathrm{d}\Omega, \end{aligned} \tag{15}$$

where $\delta_\phi \bar{J}$ is the $J'$ in Eq. (12) and based on Eq. (12) the optimization is performed.

## 3. Computation algorithm

During the optimization, the objective functional is considered to be converged when it satisfies the following criterion:

$$\frac{|J_m - J_{m-1}|}{J_{m-1}} \leq \epsilon, \tag{16}$$

where $m$ represents the step number of the optimization process.

The computation flow of the optimization is shown as follows:

(i) Initialize the value of $\phi$, $\boldsymbol{u}$ and $p$ in the design domain $D$;

(ii) Compute the flow field by the lattice kinetic scheme, save $\boldsymbol{u}$ and $p$ of all time steps;

(iii) Calculate the objective functional, if Eq. (16) and the volume constraint Eq. (2) are satisfied, terminate the optimization. Otherwise go to step (iv);

(iv) Calculate the design sensitivity and update $\phi$ using Eq. (12), then go back to step (ii) and repeat the following steps.

## 4. Numerical examples

In this section, the validity of the design sensitivity is confirmed and numerical examples of minimizing and maximizing the dissipation kinetic energy are implemented. In all the numerical examples, the Reynolds number $Re$ is defined by

$$Re = \frac{u_{\max} L}{\nu},$$

where $u_{\max}$ is the maximum velocity on $\Gamma_{\rm v}$, $L$ is the representative length of $\Gamma_{\rm v}$.

### 4.1. Validation of the design sensitivity

The validity of the design sensitivity $\delta_\phi \bar{J}$ in Eq. (15) can be confirmed if it equals to the finite difference of objective functional. Following the research by Yaji et al.,[22] we calculate the finite difference of objective functional denoted by $J'_{\rm F}$ using the central difference scheme,

$$J'_{\rm F} = \frac{\bar{J}[\chi_\phi + \epsilon_1] - \bar{J}[\chi_\phi - \epsilon_1]}{2\epsilon_1}, \tag{17}$$

where $\epsilon_1$ is a small positive variation of $\chi_\phi$. The objective is to maximize the dissipation kinetic energy of unsteady flow. The design domain is depicted in Fig. 4, which is discretized into $100\Delta x \times 100\Delta x$ lattice. A circular obstacle with the radius of $15\Delta x$ is placed at the center of the design domain and the observation nodes are chosen as the grids with coordinate of $x = 50\Delta x, y = 1\Delta x, ..., 100\Delta x$. The initial value of $\phi$ is given as $\phi = -1.0$ on the circular obstacle and the boundary of the design domain, $\phi = 1$ at the fluid field, and $\epsilon_1 = 1.0 \times 10^{-3}$. The Reynolds number is $Re = 20$. The velocity prescribed boundary $\Gamma_{\rm v}$ is at the center of the left side boundary, and the prescribed velocity is given as $\boldsymbol{u} = (U, 0)$, where $U$ is given as

$$U = \frac{4u_{\max}(y_2 - y)(y - y_1)\sin(\omega t)}{(y_2 - y_1)^2}, \tag{18}$$

and $y_1$, $y_2$ are the coordinates of the lower and upper ends of $\Gamma_{\rm v}$ on $y$-axis. $\omega$ is the angular velocity, $\omega = \frac{\pi}{25}$, which decides the change frequency of velocity. The pressure prescribed boundary $\Gamma_{\rm p}$ is at the center of right side boundary, and the prescribed pressure is given as $P = \frac{1}{3}$. The total number of the computation step of lattice kinetic scheme is $n = 4000$ steps. The observation nodes are chosen as $x = 50\Delta x, y = 0, ..., 100\Delta x$.

The finite difference approximation of the objective functional $J'_{\rm F}$ and the design sensitivity values calculated directly by the expression of $\delta_\phi \bar{J}$ at the observation nodes are compared in Fig. 5, from which one can see that the design sensitivity values calculated by the present expression show good agreement with the finite difference approximation of the objective functional confirming the validity of the proposed design sensitivity.

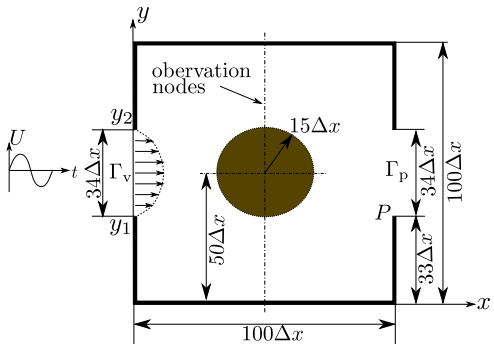


Fig. 4 The design domain for the validation of design sensitivity.

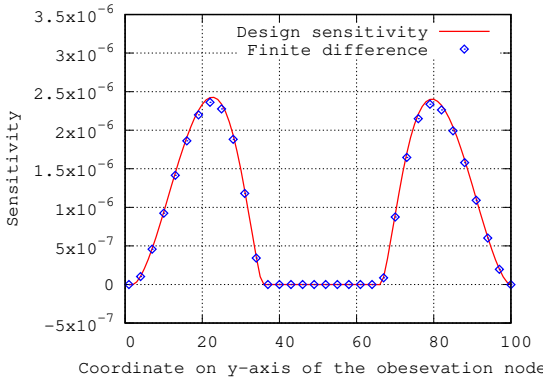


Fig. 5 Compare the design sensitivity and the finite difference of objective functional.

### 4.2. Minimizing dissipation kinetic energy

In the numerical examples of this study, the initial distribution of $\phi$ is given as $\phi_{t=0} = 1.0$ inside the design domain and $\phi_{t=0} = -1.0$ on the wall of design domain, i.e., the design domain is entirely filled of fluid at the initial step of the optimization process.

The diffuser problem aiming at minimizing the dissipation was commonly presented as a validation test case. In this study, we implement a two-dimensional diffuser example to test the proposed method, and we compare the optimization results of steady flow and unsteady flow. Also, we compare the different optimization results of minimization and maximization of dissipation. The design domain is depicted in Fig. 6 and is discretized into $100\Delta x \times 100\Delta x$ lattice points. The velocity prescribed boundary $\Gamma_{\rm v}$ is at

the left side boundary and the prescribed velocity is given as Eq. (18), where $u_{\max} = 0.01$. The pressure prescribed boundary $\Gamma_{\rm p}$ is at the center of right side boundary of design domain and $P = \frac{1}{3}$. $Re = 20$, $V_{\max} = 0.6V_0$, $V_0$ is the fluid volume at the initial step of the optimization.

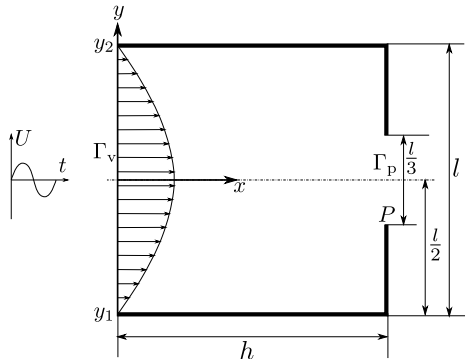


Fig. 6 Design domain for the minimization of dissipation energy.

For the unsteady case, the angular frequency is set as $\omega = \frac{\pi}{25}$ and the computation steps of lattice kinetic scheme is $n = 4000$ steps. For the steady case, the optimization is performed according to the method proposed by Yaji et al.,[20] where the objective functional is calculated when the fluid reaches a steady state after a number of steps' computation of lattice kinetic scheme, and the prescribed velocity at $\Gamma_{\rm v}$ is given as

$$U = \frac{4u_{\max}(y - y_1)(y_2 - y)}{(y_2 - y_1)^2}. \tag{19}$$

The optimized configurations of steady and unsteady fluid are shown in Fig. 7. The blue area represents the solid domain and white area represents the fluid domain. From Fig. 7, one can see that a wide channel is generated to reduce the dissipation kinetic energy in both cases. The objective $J$ and the volume $V_\Omega$ of two cases are compared in Table 1, where $J_0$ and $V_0$ denote the objective and volume computed at the initial step of the optimization. Comparing the objective value, we find that the dissipation is reduced efficiently in the optimization for unsteady case, where a wider and straight flow channel is generated to reduce the dissipation.[1]

Table 1: The values of the objective and volume of minimizing the dissipation kinetic energy

| | Objective value ($J/J_0$) | Volume ($V_\Omega/V_0$) |
|---|---|---|
| Steady | 2.80 | 54.56% |
| Unsteady | 0.56 | 51.64% |

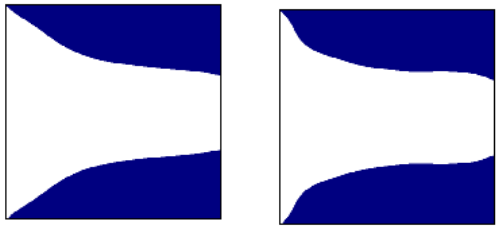

(a) Steady (b) Unsteady

Fig. 7 Optimized configurations of minimizing the dissipation energy.

### 4.3. Maximizing dissipation kinetic energy

In this section, numerical examples of maximizing the dissipation of the kinetic energy are implemented. The design domain is the same as that of Section 4.2 and is discretized into $100\Delta x \times 100\Delta x$ lattice. Same values are given for these parameters as in Section 4.2: the volume constraint $V$, prescribed velocity $U$ at $\Gamma_{\rm v}$, prescribed pressure $P$ at $\Gamma_{\rm p}$, computation step number $n$, inflow frequency $\omega$ and the Reynolds number $Re$.

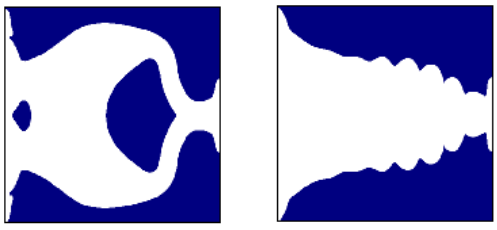

(a) Steady (b) Unsteady

Fig. 8 Optimized configurations of maximizing the dissipation energy.

Fig. 8(a) shows the optimized configuration for the steady flow, where the flow channel is divided to narrow channels by solid material. Fig. 8(b) shows the optimized configuration for the unsteady flow, in which islands are generated along the boundary of flow channel. The configurations at different iterations during the optimization of the steady case are shown in Fig. 9(a), and the configurations of the unsteady case are shown in Fig. 9(b). Fig. 9 shows that the solid material is generated firstly near the boundary $\Gamma_{\rm p}$ to prevent the fluid from flowing out directly, helping increase the dissipation.

The distribution of the dissipation energy at the initial and final iteration steps are shown in Fig. 10, where Fig. 10(a) is for the steady case and Fig. 10(b) for the unsteady case.

The value of the objective $J$ and the volume $V_\Omega$ are shown in Table 2, from which one can see that the dissipation energy is increased in the steady and unsteady case, and the

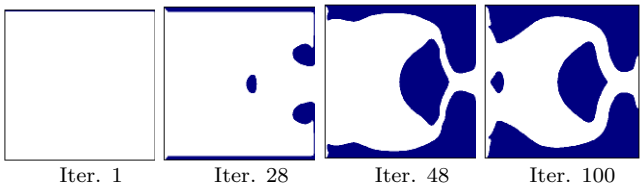


(a) Steady

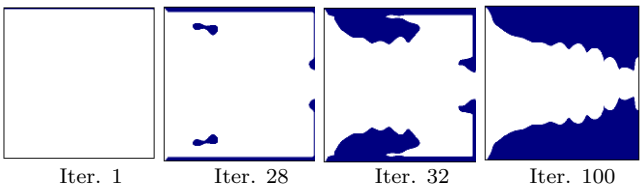


(b) Unsteady

Fig. 9 Configurations at different iterations

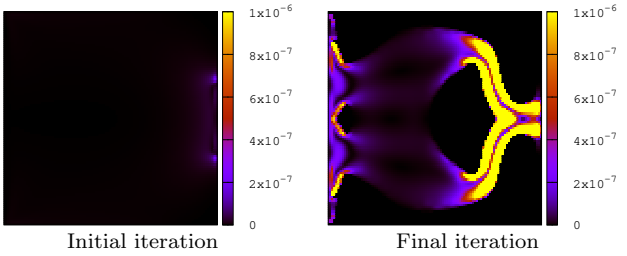


(a) Steady case

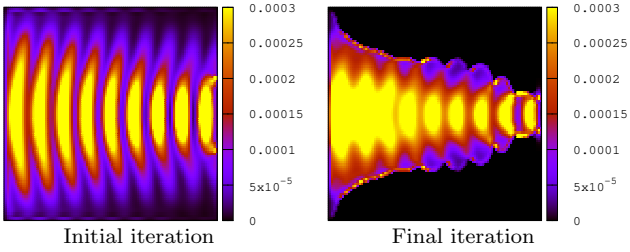


(b) Unsteady case

Fig. 10 Distribution of the dissipation kinetic energy in cases of maximizing dissipation.

increasing rate of objective value for the steady case is much greater than that of the unsteady case. In the optimized configuration of steady flow case, the generated solid materials divide the flow to narrow streams in the optimized configuration, which can increase the velocity shear. Since the dissipation energy is formulated by velocity shear, the dissipation energy is greatly increased in the optimized configuration.

**4.4. Dependence of the results on the inflow frequency**

In this section, the influence of the inflow frequency is discussed. The design domain is depicted in Fig. 11 and is discretized into $100\Delta x \times 100\Delta x$ lattice. The velocity prescribed boundary $\Gamma_{\mathrm{v}}$ and the pressure prescribed boundary $\Gamma_{\mathrm{p}}$ are located at the center of left and right side boundaries, respectively. The velocity on $\Gamma_{\mathrm{v}}$ is given as

$$U = \frac{4u_{\max}(y-y_1)(y_2-y)\cos(\omega t)}{(y_2-y_1)^2}, \tag{20}$$

where $u_{\max} = 0.01$. The pressure on $\Gamma_{\mathrm{p}}$ is $P = \frac{1}{3}$, and $V_{\max} = 0.6V_0$, $Re = 20$ and $n = 7200$. Numerical examples for different values of $\omega$: $\omega = \frac{\pi}{50}, \frac{\pi}{100}$ and $\frac{\pi}{150}$ are presented.

Table 2: Objective and volume value of maximizing dissipation kinetic energy

| | Objective value $(J/J_0)$ | Volume $(V_\Omega/V_0)$ |
|---|---|---|
| Steady | 104.03 | 51.06% |
| Unsteady | 1.12 | 49.90% |

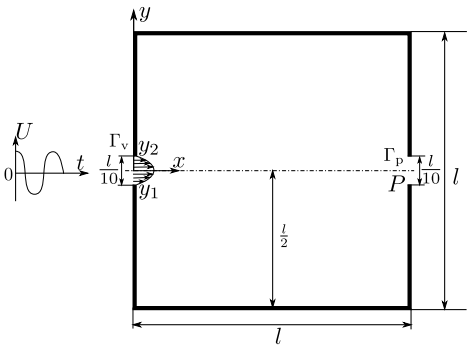


Fig. 11 The design domain of the examples for different $\omega$.

The optimized configurations are shown in Fig. 12, where Fig. 12(a) is for $\omega = \frac{\pi}{50}$, Fig. 12(b) for $\omega = \frac{\pi}{100}$ and Fig. 12(c) for $\omega = \frac{\pi}{150}$. Fig. 12 shows that the boundaries of the channel become simple against the increase of $\omega$. The values of the objective and the volume are compared in Table 3, from which we find that the objective value increases against the decrease of $\omega$.

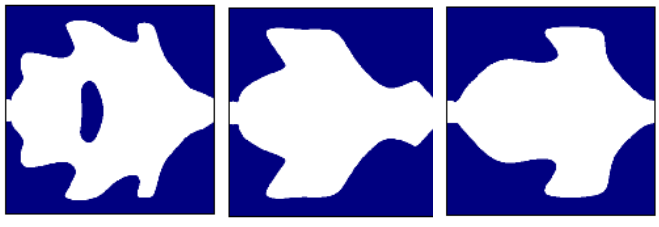

(a) $\omega = \frac{\pi}{50}$ (b) $\omega = \frac{\pi}{100}$ (c) $\omega = \frac{\pi}{150}$

Fig. 12 Optimized configurations of different $\omega$.

Table 3: The values of the objective and volume in numerical examples for different $\omega$

| $\omega$ | Objective value ($J/J_0$) | Volume ($V_\Omega/V_0$) |
|---|---|---|
| $\frac{\pi}{50}$ | 1.22 | 52.86% |
| $\frac{\pi}{100}$ | 1.85 | 47.90% |
| $\frac{\pi}{150}$ | 2.27 | 47.80% |

The distribution of the dissipation of the kinetic energy at the initial and final iteration steps for three cases are shown in Fig. 13. The kinetic energy is dissipated mostly near the velocity prescribed boundary $\Gamma_v$. The kinetic energy is dissipated soon after it enters the cavity.

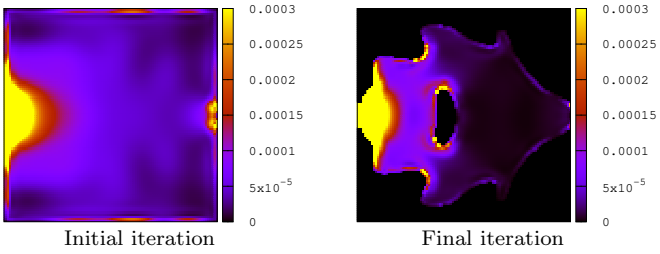


(a) $\omega = \frac{\pi}{50}$

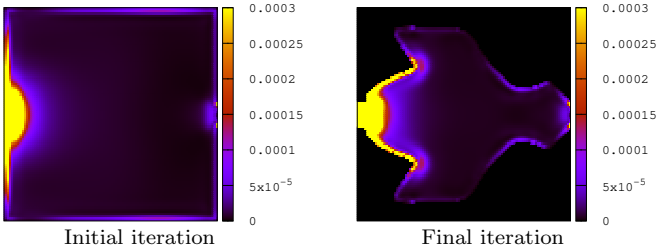


(b) $\omega = \frac{\pi}{100}$

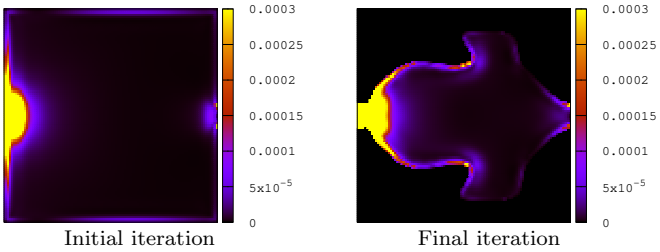


(c) $\omega = \frac{\pi}{150}$

Fig. 13 Distribution of the dissipation of the kinetic energy.

### 4.5. Dependence of the results on the Reynolds number

We now test the influence of the Reynolds number on the optimization results. The design domain is depicted in Fig. 14, and is discretized into $100\Delta x \times 100\Delta x$ lattice. The velocity prescribed boundary $\Gamma_v$ is at the center of the left side bounday, and the prescribed velocity is given by Eq. (20), where $u_{\max} = 0.05$. The pressure prescribed boundary $\Gamma_p$ is at the center of the right side boundary, and $P = \frac{1}{3}$. $V_{\max} = 0.7V_0$, $n = 7200$ and $\omega = \frac{\pi}{50}$. Numerical examples of different Reynolds number: $Re = 20, 50, 100$, are presented.

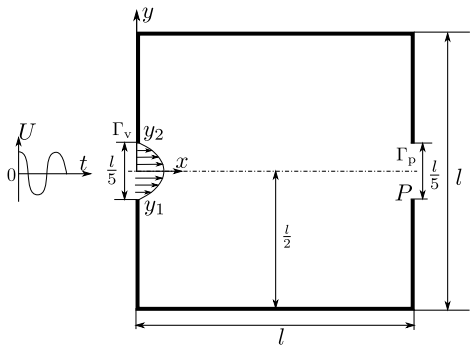


Fig. 14 The design domain of examples for different Reynolds number.

The optimized configurations are shown in Fig. 15, Fig. 15(a) for $Re = 20$, Fig. 15(b) $Re = 50$ and Fig. 15(c) for $Re = 100$. From Fig. 15, we find that the boundary size of concavity and extrusion of the channels becomes slightly smaller against the increasing of $Re$, and this can be explained that flow of a higher Reynolds number has a stronger inertial force, hence, it is difficult for a change in the velocity of flow.

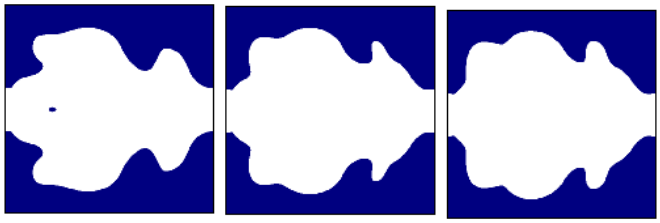

(a) $Re = 20$ (b) $Re = 50$ (c) $Re = 100$

Fig. 15 Optimized configurations of different Reynolds number.

### 5. Conclusions

This study proposes a topology optimization method for maximizing the dissipation of kinetic energy of incompressible unsteady Navier-Stokes fluid using the lattice kinetic scheme. The adjoint equation of lattice kinetic scheme and design sensitivity for unsteady flow are derived. The validity of the design sensitivity and the utility of the optimization method are demonstrated through some numerical examples. This research can be applied to the structure design of hydraulic anti-vibration devices.

**References**


(1) Borrvall, M. and Petersson, J., Topology optimization of fluids in Stokes flow, *International journal for numerical methods in fluids*, Vol. 41, No. 1, pp. 77–107, 2003.

(2) Gersborg-Hansen, A., Sigmund, O. and Habor, R., Topology optimization of channel flow problems, *Structural and Multidisciplinary Optimization*, Vol. 30, pp. 181–192, 2004.

(3) Andreasen, C.S., Gersborg, A.R. and Sigmund, O., Topology optimization of microfluidic mixers, *International journal for numerical methods in fluids*, Vol. 61, No. 5, pp. 498–513, 2009.

(4) Makhijia, D., Pingen, G., Yang, R. and Maute, K., Toplogy optimization of multi-component flows using a multi-relaxation time lattice Boltzmann emthod, *Computers and Fluids*, Vol. 67, pp. 104–114, 2012.

(5) Pingen, G., Evgrafov, A. and Maute, K., Toplogy optimization of flow domains using the lattice Boltzmann method, *Structural and Multidisplinary Optimization*, Vol. 34, pp. 507–524, 2007.

(6) Kreissl,S., Pingen, G. and Maute, K., An explicit level set approach for generalized shape optimization of fluids with the lattice Boltzmann method, *International Journal for Numerical Methods in Fluids*, Vol. 65, pp. 496–519, 2009.

(7) Pingen, G. and Maute, K., Optimal design for non-Newtonian flows using a topology optimization approach, *Computers and Mathematics with Applications*, Vol. 59, pp. 2340–2350, 2010.

(8) Inamuro, T., A lattice kinetic scheme for incompressible viscous flows with heat transfer, *Philosophical transactions of the Royal society A*, Vol. 360, pp. 477–484, 2002.

(9) Sone, Y., Notes on kinetic-equation approach of fluid-dynamic equations, Department of Mechanics, Royal Institute of Technology, Stockholm, 2000.

(10) Junk, M. and Raghurama Rao, S.V., A New Discrete Velocity Method for Navier-Stokes Equations, *Journal of Computational Physics*, Vol. 155, No. 1, pp. 178–198, 2010.

(11) Succi, S., The lattice Boltzmann equation for fluid dynamics and beyond, *Oxford University Press*, 2010.

(12) He, X. and Luo, L.S., Lattice Boltzmann model for the incompressible Navier-Stokes equation, *Journal of statistical physics*, Vol. 88, pp. 927–944, 1997.

(13) Kreissl, S., Pingen, G. and Maute, K., Topology optimization for unsteady flow, *International Journal of Numerical Methods in Engineering*, Vol. 87, No. 13, pp. 1229–1253, 2011.

(14) Deng, Y., Liu, Z., Zhang, P., Liu, Y. and Wu, Y., Topology optimization of unsteady incompressible Navier-Stokes flows, *Journal of Computational Physics*, Vol. 230, No. 17, pp. 6688–6708, 2011.

(15) Nørgaard, S., Sigmund, O. and Lazarov, B., Topology optimization of unsteady flow problems using the lattice Boltzmann method, *Journal of Computational Physics*, Vol. 307, No. 17, pp. 291–307, 2016.

(16) Chen, C., Yaji, K., Yamada, T., Izui, K. and Nishiwaki, S., Local-in-time adjoint-based topology optimization of unsteady fluid flows using the lattice Boltzmann method, *Mechanical Engineering Journal*, Vol. 4, No. 3, pp. 17-00120-17-00120, 2017.

(17) Nguyen, T., Isakari, H., Takahashi, T., Yaji, K., Yoshino. M. and Matsumoto, T, Level-set based topology optimization of transient flow using lattice Boltzmann method considering an oscillating flow condition, *Computers and Mathematics with Applications*, Vol. 80, pp. 82–108, 2020.

(18) Lin, S., Zhao, L., Guest, J.K., Weihs, T.P. and Liu, Z., Topology Optimization of Fixed-Geometry Fluid Diodes, *Journal of Mechanical Design*, Vol. 137, No. 8, 2015.

(19) Sato, Y., Yaji, K. and Izui, K., Topology optimization of a no-moving-part valve incorporating Pareto frontier exploration, *Structural Multidisciplinary Optimization*, Vol. 56, pp. 839–851, 2017.

(20) Yaji, K., Yamada, T., Yoshino, M. and Matsumoto, T., Topology optimization using the lattice Boltzmann method incorporating level set boundary expressions, *Journal of Computational Physics*, Vol. 274, pp. 158–181, 2014.

(21) Yamada,T., Izui, K., Nishiwaki, S. and Takezawa, A, A topology optimization method based on the level set method incorporating a fictitious interface energy, *Computer Methods in Applied Mechanics and Engineering*, Vol. 199, pp. 2876–2891, 2010.

(22) Yaji,K., Yamada, T., Yoshino, M. and Matsumoto,T., Topology optimization in thermal-fluid flow using the lattice Boltzmann method, *Journal of Computational Physics*, Vol. 307, pp. 355–377, 2016.